Indian Journal of Chemistry
Vol. 59A, May 2020, pp. 646-651

# Morphology-dependent photocatalytic activity of $TiO_2$ crystals

Guowei Wang[a], Hongguang Zhang[b,*], Meng Wang[c], Yu Wang[d], Chunhui Xia[b], Shuang Fu[b] & Feng Xu[b]

[a] College of Pathology, Qiqihar Medical University, Qiqihar 161006, PR China

[b] College of Pharmacy, Qiqihar Medical University, Qiqihar 161006, PR China

[c] College of Adult and Continuing Education, Qiqihar Medical University, Qiqihar 161006, PR China

[d] College of Basic Medicine, Qiqihar Medical University, Qiqihar 161006, PR China

E-mail: zhanghg@qmu.edu.cn

*Received 30 August 2019; revised and accepted 20 April 2020*

$TiO_2$ crystals with different morphologies have been successfully synthesized by simple hydrothermal method. All samples are characterized carefully by XRD, SEM, TEM, and BET techniques and the morphological effect on the photocatalytic activity of the obtained $TiO_2$ crystals has been evaluated by degrading the pollutant molecules. The experimental results show that the $TiO_2$ samples with different morphologies exhibited different activities to pollutant degradation. The core-shell spheres have exhibited the best photocatalytic activity, with the almost complete degradation of methyl orange (MO) and rhodamine B within 15 min under UV-light irradiation. After 20 min UV-light irradiation, the degradation efficiency of the MO solution is about 68.9%. It can be concluded that a morphological effect is responsible for the photocatalytic performance. The crystals with large BET surface area, the small crystallite size shows the better the photocatalytic performance.

**Keywords:** $TiO_2$, Hydrothermal method, Different morphologies, Photocatalytic activity

Photocatalytic degradation of metal oxide semiconductor materials has become one of the most intensive areas of research during recent years[1]. In particular, the problem of environmental pollution and energy shortage has received considerable critical attention. The photocatalytic method is considered to be a promising method for the removal of environment pollutants[2]. Recently, great efforts have been made to design and develop the highly efficient semiconductor photocatalysts, such as $TiO_2$[3,4], $CdS$[5], $ZnO$[6], $BiVO_4$[7], $MoS_2$[8], $CeO_2$[9], $Cu_2O$[10], $Fe_2O_3$[11], and $SnO_2$[12] etc. Among the various types of semiconductor, $TiO_2$ (titanium dioxide) is one of the most promising materials for photocatalytic applications[13]. It has outstanding mechanical strength, high thermal and chemical stabilities, low cost, good optical, electronic, and excellent catalytic properties[14-16]. As we know, the photocatalytic activity of $TiO_2$ depends on its surface area, crystallite size, crystal phase and crystallinity[17]. Thus, it is highly desirable to develop a generalized and efficient strategy to synthesize $TiO_2$ with high photocatalytic activity.

To date, a wide variety of $TiO_2$ have been developed including nanorods, nanoparticles, nanodisks, nanotubes, nanowires, nanocages, nanoflowers, thin films, microspheres, core-shell spheres, hollow spheres, and so on. The nanostructures of $TiO_2$ can be tuned by careful selection of the experimental parameters and synthesis technology. For example, Weon *et al*. reported that the doubly open-ended $TiO_2$ nanotubes exhibited high activity and durability for the photocatalytic degradation of gaseous acetaldehyde and toluene[18]. Tsuji *et al*. found that the $Au/TiO_2$ photocatalysts showed enhanced methyl orange (MO) degradation rates in neutral and acidic solutions[19]. Jia *et al*. demonstrated that the $TiO_2$ hollow boxes with hierarchical structures exhibited an excellent performance in the photocatalytic degradation of organic pollutant methylene blue [20]. Although photocatalytic degradation by using $TiO_2$ has achieved great progress for the removal of environment pollutants, nevertheless, there are few literatures that concerned the shape of $TiO_2$ nanostructure on their photocatalytic properties.

In this work, $TiO_2$ with three different morphologies (nanorod, core-shell sphere and flower sphere) have been successfully prepared by hydrothermal method. The photocatalytic activities of the as-fabricated samples were evaluated by decomposing methyl orange (MO), rhodamine B (RhB) and phenol under UV-light irradiation. Compared with $TiO_2$ nanorod, $TiO_2$ flower sphere, and P25-$TiO_2$, $TiO_2$ core-shell sphere was found to have the best photocatalytic activity towards pollutant degradation. The results show that $TiO_2$ exhibits morphology-dependent photocatalytic activities.

## Materials and Method

### Reagents and materials

Titanium sulfate ($Ti(SO_4)_2$), ethylenediamine tetraacetic acid (EDTA), citric acid ($C_6H_8O_7 \cdot H_2O$), ethanediamine ($C_2H_8N_2$), and hydrofluoric acid (HF) were obtained from Sinopharm Chemical Reagent Co., Ltd. All reagents were A.R. grade and used without further purification.

### Synthesis of $TiO_2$ core-shell sphere, $TiO_2$ nanorod, and $TiO_2$ flower sphere

All of the samples were prepared by hydrothermal method. $TiO_2$ core-shell sphere ($TiO_2$-C): 0.2400 g of $Ti(SO_4)_2$ and 1.461 g of EDTA were dissolved in 30 mL $H_2O$ by stirring. $TiO_2$ nanorod ($TiO_2$-N): 0.2400 g of $Ti(SO_4)_2$ and 0.063 g of $H_3Cit$ ($C_6H_8O_7 \cdot H_2O$) were dissolved into 24 mL of $H_2O/C_2H_5OH$ mixed solvent (7:5, v/v) by stirring. Subsequently, 8.0 ml of ethanediamine was dropwise added into the above solution. $TiO_2$ flower sphere ($TiO_2$-F): 0.2400 g of $Ti(SO_4)_2$ and 0.063 g of $H_3Cit$ were dissolved into 12.8 mL of $H_2O$ by stirring. Subsequently, 8 ml of ethanediamine, 10 mL of $C_2H_5OH$, and 1.2 mL of HF were added into the above solution in turn. After that, the three mixed solution were transferred into three Teflon lined autoclave of 50 mL capacity and kept in an oven at 180 °C for 8 h. After reaction, the precipitates were collected, washed with deionized water and absolute ethanol for 3 times, and dried at 60 °C for 12 h in air.

### Characterization techinques

The crystal phase of all the samples were recorded using X-ray diffractometer (XRD) (XRD-6000, Shimadzu) equipped with Cu Kα radiation (λ = 1.5406 Å) in the 2θ range from 10° to 70°. Scanning electron microscope (SEM) equipped with an energy-dispersive X-Ray spectrometer (EDX) (S-4800, Hitachi) and transmission electron microscope (TEM) (Tecnai G2 S-Twin, FEI) were used to characterize the morphology and size of all the samples. The specific surface areas were calculated by a Brunauer-Emmett-Teller (BET) specific surface analysis device (ASAP 2010, Micromeritics). The optical absorption spectra of targeted pollutants were recorded by a UV-visible spectrophotometer (UV-1750, Shimadzu). Concentration of chemical oxygen demand (COD) was determined by using HACH DR2800 spectrophotometer.

### Photocatalytic experiments

The photocatalytic activities of the samples ($TiO_2$ core-shell sphere, $TiO_2$ nanorod, $TiO_2$ flower sphere, and P25-$TiO_2$) were evaluated with MO as targeted pollutant. Generally, 10 mg of the sample was placed into a MO aqueous solution (40 mL, 20 $mg \cdot L^{-1}$). Before the irradiation, the mixed solution was stirred in the dark for 60 min to achieve a saturated adsorption. A 500 W mercury lamp was used as the UV-light source. 2 mL of suspension were taken out at a given time interval. Subsequently, the absorbance spectra of MO solutions were analyzed by a UV-visible spectrometer. Additionally, when phenol aqueous solution (40 mL, 20 $mg \cdot L^{-1}$) or RhB aqueous solution (40 mL, 20 $mg \cdot L^{-1}$) was used as targeted pollutant, we used a process which was similar to that described above.

## Results and Discussion

The structure and composition of the P25-$TiO_2$, $TiO_2$-C, $TiO_2$-F, and $TiO_2$-N were investigated by XRD (Fig. 1). For the XRD pattern of the P25-$TiO_2$, two diffraction peaks at 27.5, and 36.1° were assigned to the (110), and (101) crystal planes of rutile $TiO_2$ (JCPDS, No. 73-1765), all other diffraction peaks could be indexed to anatase $TiO_2$ (JCPDS, No. 21-1272). The result showed that P25-$TiO_2$ contained anatase and rutile crystalline phases. As for the $TiO_2$-C, $TiO_2$-F, and $TiO_2$-N samples, all of the characteristic peaks could be well indexed as a pure anatase $TiO_2$ (JCPDS, No. 21-1272). The average crystallite size of the sample was estimated using the Debye-Scherrer's equation: $D=0.89\lambda/(\beta\cos\theta)$, where D is the average grain size, λ is the X-ray wavelength

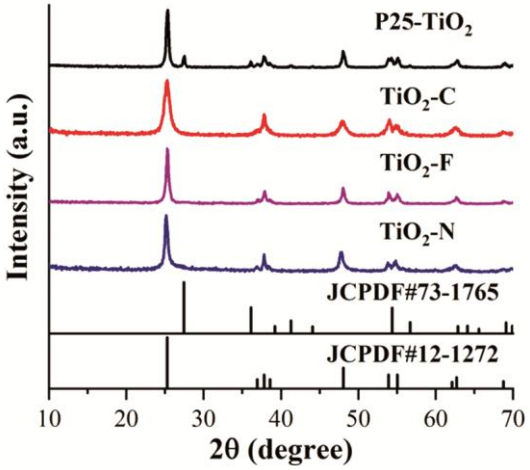


Fig. 1 — XRD patterns of the as-formed $TiO_2$-C, $TiO_2$-N, $TiO_2$-F, and P25-$TiO_2$.

(0.15405 nm), β and θ are the full-width at half maximum and diffraction angle, respectively. Thus, the average crystallite sizes of the $TiO_2$-C, $TiO_2$-F, $TiO_2$-N, and P25-$TiO_2$ were estimated to be approximately 11.82, 22.68, 12.78, and 21.19 nm, respectively.

The morphologies of the $TiO_2$-C, $TiO_2$-N, $TiO_2$-F, and P25-$TiO_2$ were investigated by SEM. As showed in Fig. 2a, we can see that the $TiO_2$-C sample shows a core-shell structure with diameter of 0.5-1.5 μm. In Fig. 2b, the morphology of the $TiO_2$-N sample is highly uniform nanorods with an average diameter of 460 nm. Fig. 2c shows SEM image of the $TiO_2$-F sample, clearly exhibiting that the sample is composed of flower spheres with a diameter of about 1-2 μm. Furthermore, it is obvious from Fig. 2d that the P25-$TiO_2$ is composed of nanoparticles with diameters of 30-40 nm. Interestingly, when different reagents were added into the system, including EDTA, ethanediamine, and HF, the morphologies of the $TiO_2$ samples were significantly different. This phenomenon occurs because they can be selectively adsorbed on different crystal faces of $TiO_2$ during the growth of crystal, which results in different growth rates on different crystal faces. Therefore, $TiO_2$ samples exhibited significantly different morphologies during anisotropic growth.

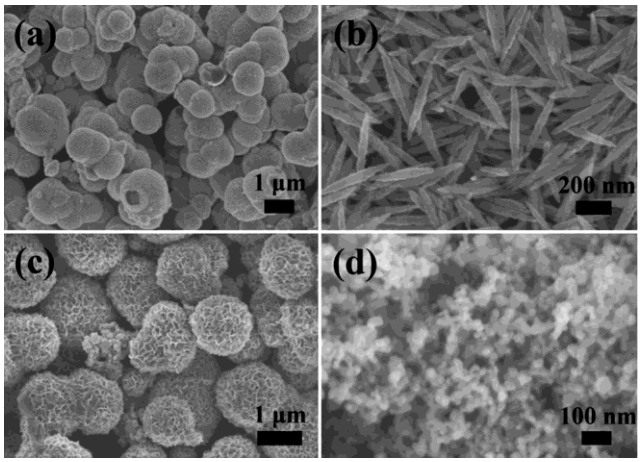


Fig. 2 — SEM images of (a) $TiO_2$-C, (b) $TiO_2$-N, (c) $TiO_2$-F, and (d) P25-$TiO_2$.

The morphologies of the $TiO_2$-C, $TiO_2$-N, and $TiO_2$-F were further examined using TEM as illustrated in Fig. 3. The TEM images of three samples describe the similar structure as observed by the SEM images. From Fig. 3a, the core-shell structure of the $TiO_2$-C can be confirmed by light and dark contrast. For $TiO_2$-N (Fig. 3b), the sample exhibits an obviously ordered nanorod structure. The TEM image of the $TiO_2$-F reveals that it consists of solid flower spheres (Fig. 3c), which is consistent with the result shown in the SEM image. The chemical compositions of three samples were analyzed by EDX spectroscopy (Fig. 3d-3f). The EDX results confirmed that all of the three samples were composed of titanium (Ti) and oxygen (O), which was in excellent agreement with the XRD analysis.

The surface areas of the $TiO_2$-C, $TiO_2$-N, $TiO_2$-F were also measured by using nitrogen adsorption/desorption isotherms. The $N_2$ adsorption/desorption isotherms displayed in Fig. 4 shows the type III behavior with a distinct H3 hysteresis loop in the range of 0.8-1.0 $P/P_0$ according

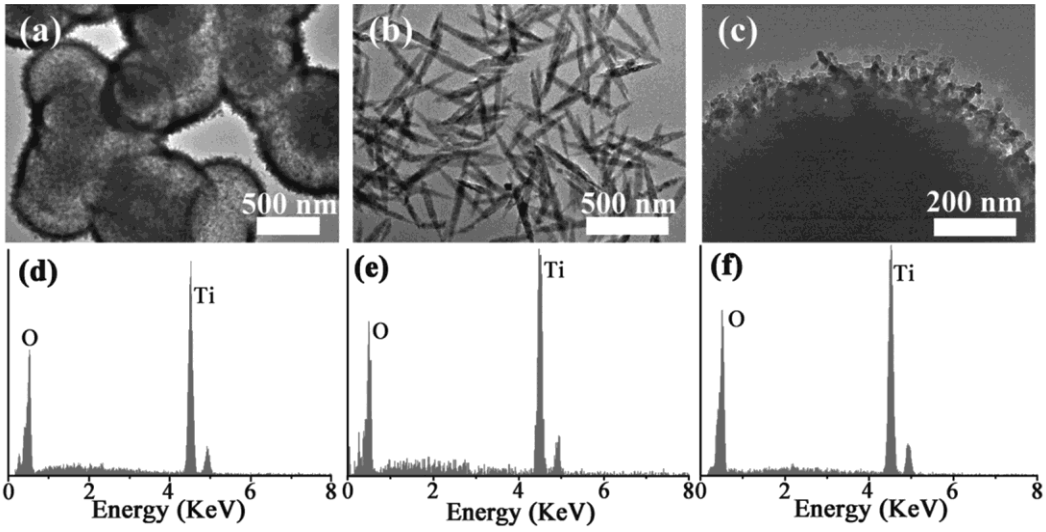


Fig. 3 — TEM images and energy dispersive X-ray spectra (EDX) of (a, d) $TiO_2$-C, (b, e) $TiO_2$-N, and (c, f) $TiO_2$-F.

to the IUPAC classification[21]. The Brunauer-Emmett-Teller (BET) specific surface area, crystallite size, and crystal phase of the different samples are listed in Table 1. As shown in Table 1, the specific surface area of the $TiO_2$-C, $TiO_2$-N, $TiO_2$-F, and P25-$TiO_2$ is 134.32, 54.18, 32.10, and 50.00 $m^2/g$[22], respectively. The specific surface area of $TiO_2$-C is the largest among the four samples, which will absorb more catalyst and provide more surface active sites.

The photocatalytic activities of the four samples were evaluated by the degradation of MO under UV-light irradiation. Prior to the photocatalytic test, all samples took 60 min to reach adsorption saturation in the dark. As can be seen in Fig. 5a, MO shows nearly no change in the absorption intensity upon UV-light irradiation in the absence of any catalyst. The $TiO_2$-C has shown significantly enhanced photocatalytic ability in contrast to other samples under UV-light irradiation at the same time. It can be seen that $TiO_2$-C could rapidly remove MO from the solutions and the removal efficiency could reach up to 93.4% within 10 min, and the MO aqueous solution could be completely decomposed in 15 min. However, for P25-$TiO_2$, $TiO_2$-N, and $TiO_2$-F samples, the photodegradation efficiency of MO aqueous solution was 84.3%, 27.2%, and 18.8% after 20 min, respectively. It is now well established that the photocatalytic activity of a catalyst is dependent on its specific surface area, crystallite size, and crystal phase[17,23,24]. Thus, the excellent photocatalytic ability may be due to the cause that the $TiO_2$-C has larger specific surface area (134.32 $m^2/g$) and smaller crystallite size (11.82 nm). The large specific surface area of the photocatalyst can provide more surface active sites and adsorb more pollutant molecules on its surface. Besides, the small crystallite size of the photocatalyst can maximize the number of active sites. Those factors cause an increase in photocatalytic performance. Compared with the $TiO_2$-C, although the P25-$TiO_2$ has lower surface area (50.00 $m^2/g$) and larger crystallite size (21.19 nm) (Table 1), the relatively high photocatalytic ability is due to the $e^-$ and $h^+$ could be effectively separated in rutile–anatase heterojunction[25]. Fig. 5c shows the kinetic curves of the photodegradation of MO using the plot of $\ln(C_0/C)$ versus illumination time. It can be seen that the highest activity was found for $TiO_2$-C sample, with a degradation constant rate of 0.2179 $min^{-1}$. To further test the conclusions obtained from the above analyses, we also performed the degradation experiment of RhB solution under the same conditions. As shown in Fig. 5b and 5d, $TiO_2$-C sample displayed better degradation efficiency of RhB solution than other samples under UV-light illumination and possessed a maximum rate constant of 0.2554 $min^{-1}$. This result further proved the high photocatalytic activity of $TiO_2$-C sample.

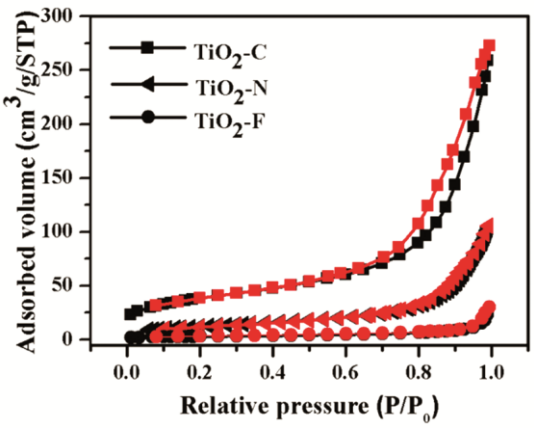


Fig. 4 — Nitrogen adsorption/desorption isotherms of $TiO_2$-C, $TiO_2$-N, and $TiO_2$-F.

Table 1 — Summary of BET surface area, crystallite size, and crystal phase of the different samples

| Sample | crystallite size (nm) | BET surface area ($m^2/g$) | crystal phase |
|---|---|---|---|
| $TiO_2$-C | 11.82 | 134.32 | anatase |
| $TiO_2$-N | 12.78 | 54.18 | anatase |
| $TiO_2$-F | 22.68 | 32.10 | anatase |
| P25-$TiO_2$ | 21.19 | 50.00 | anatase-rutile |

We also investigated the changes in pH and COD before and after the degradation of MO solutions in the presence of $TiO_2$-C photocatalyst. As shown in Fig. 6a, we can see that the pH value of the MO solution decreased from 5.4 to 4.8 after degradation. After 20 min UV-light irradiation, the COD concentration of the MO solution decreased from the initial 76.3 mg/L to the final 23.7 mg/L, which confirmed that the MO solution was photodegraded by the $TiO_2$-C photocatalyst. Furthermore, the dosage of catalyst is a key factor in its practical application. It can be seen that the more amount of $TiO_2$-C catalyst used, the greater degradation efficiency of MO solution it would show (Fig. 6b). After 20 min UV-light irradiation, we found that the photodegradation rates of MO solution were 98.6%, 97.8%, 80.3%, and 57.9% when the dosages of $TiO_2$-C catalyst were 12 mg, 10 mg, 8 mg, and 5 mg, respectively. After comprehensive consideration of the catalytic

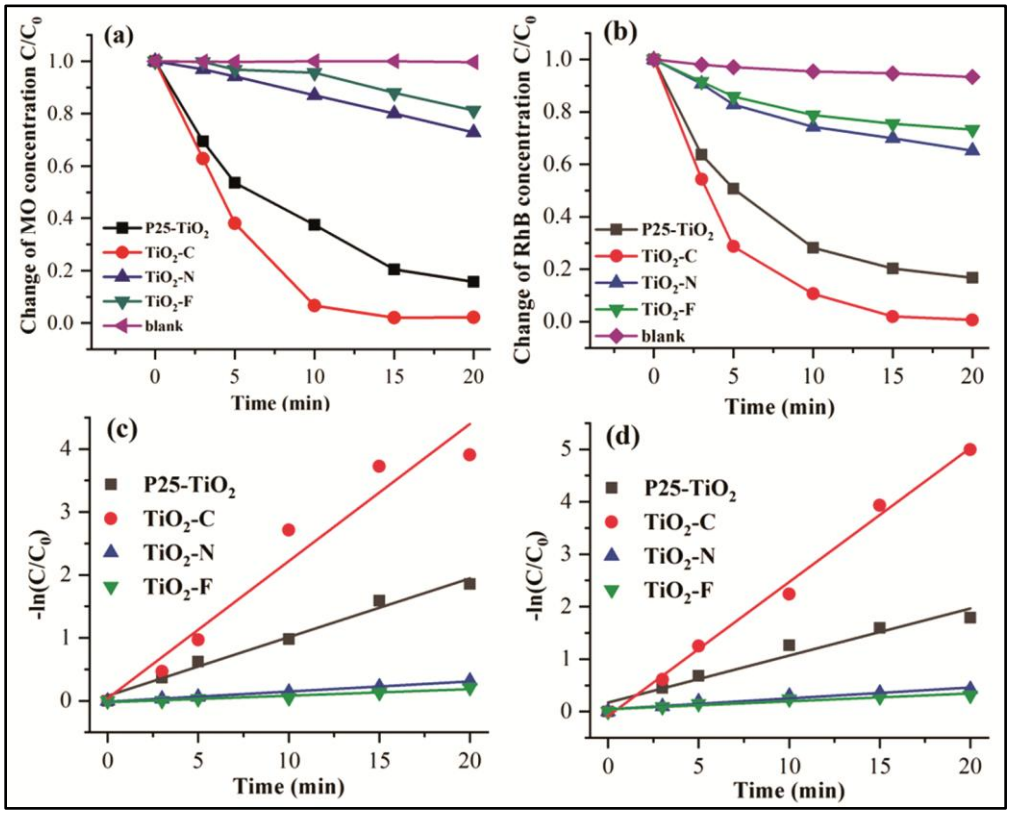


Fig. 5 — Photodegradation plots of (a) MO and (b) RhB by different photocatalysts under UV-light irradiation. First-order plots for the photodegradation of (c) MO and (d) RhB using different photocatalysts.

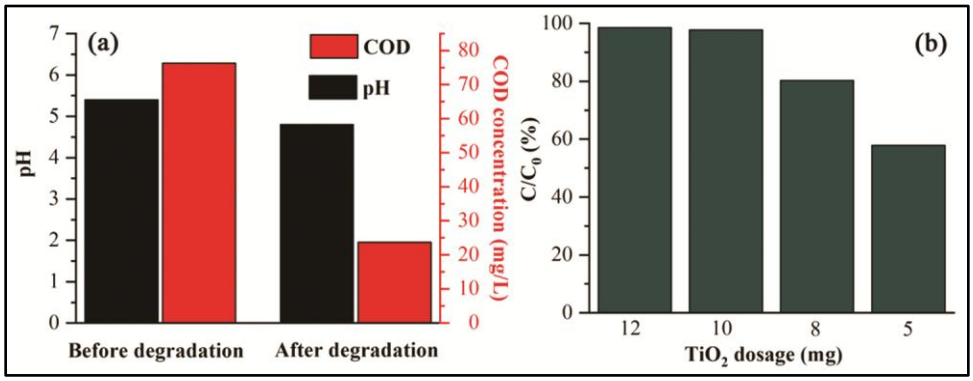


Fig. 6 — Graphs for (a) the change in pH and COD of MO solution before and after degradation using $TiO_2$-C catalyst and (b) photodegradation of MO in the presence of different dosages of $TiO_2$-C catalyst.

efficiency and cost of catalyst, we think that the optimal addition amount of $TiO_2$-C catalyst is 10 mg.

In order to further explore the photocatalytic properties of the $TiO_2$-C, we continued the same test by dispersing the $TiO_2$-C and P25-$TiO_2$ into a phenol solution (20 mg/L), and the results are shown in Fig. 7. As shown in Fig. 7a, the degradation of phenol solution can be hardly observed in the absence of catalyst. Here we found that the P25-$TiO_2$ has poor photocatalytic activity and only 8.2% phenol was degraded after 60 min UV-light irradiation, while the $TiO_2$-C exhibited better photocatalytic activity and the degradation rate of the phenol solution was 32.4% in 60 min. This result also further demonstrates the superiority of $TiO_2$-C catalysts for the photocatalytic process. The time-dependent absorption spectra of the phenol solution during the irradiation are displayed in Fig. 7b. We can see that the maximum absorbance of the phenol solution decreases greatly after UV-light irradiation within 60 min for the $TiO_2$-C.

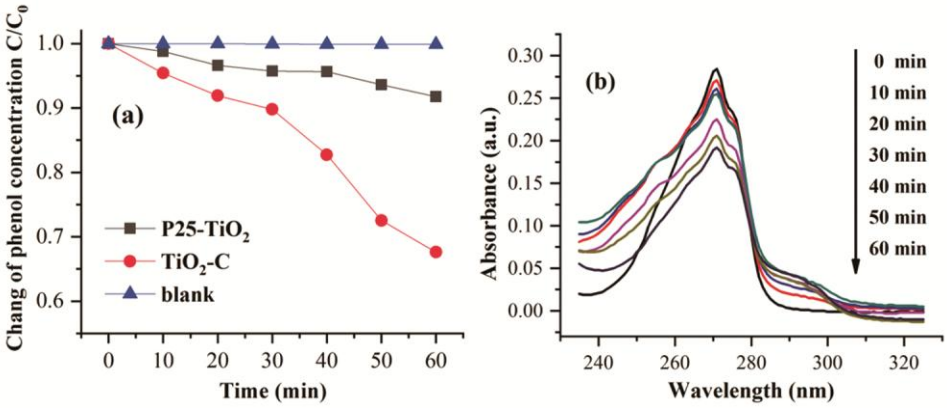


Fig. 7 — (a) Photodegradation plots of phenol by $TiO_2$-C and P25-$TiO_2$ under UV-light and (b) the absorption spectra of the aqueous phenol solution with different irradiation time in the presence of the $TiO_2$-C.

## Conclusions

In conclusion, a series of $TiO_2$ crystals with various morphologies were synthesized by hydrothermal method. Detailed morphology analysis implies that the core-shell spherical, rod-like, and flower-like $TiO_2$ crystals were generated. The different morphologies of $TiO_2$ photocatalysts exhibited distinct photocatalytic activities. As a result, the resulting $TiO_2$ core-shell spheres exhibited higher activity for pollutant degradation relative to the $TiO_2$ nanorods, $TiO_2$ flower spheres, and P25-$TiO_2$, which may be attributed to its larger surface area and smaller crystallite size. Thus, we conclude that the morphology of the $TiO_2$ crystals can affect its photocatalytic activity. This provides a useful strategy to design and fabricate highly efficient photocatalysts.

## Acknowledgment

This work is financially supported by the University Nursing Program for Young Scholars with Creative Talents in Heilongjiang Province (Grant No. UNPYSCT-2018028).

### References

1 Chan S H S, Yeong Wu T, Juan J C & Teh C Y, *J Chem Techno Biotechno*, 86 (2011) 1130.
2 Hoffmann M R, Martin S T, Choi W & Bahnemann D W, *Cheml Rev*, 95 (1995) 69.
3 Fakhrutdinova E, Shabalina A, Svetlichnyi V & Salanov A, *J Chem Res*, 12 (2016) 729.
4 Kite S, Sathe D, Kadam A, Chavan S & Garadkar K, *Res on Chem Intermed*, 46 (2020) 1255.
5 Cheng L, Xiang Q, Liao Y & Zhang H, *Energy Environ Sci*, 11 (2018) 1362.
6 Ong C B, Ng L Y & Mohammad A W, *Renewable Sustainable Energy Rev* 81 (2018) 536.
7 Petala A, Noe A, Frontistis Z, Drivas C, Kennou S, Mantzavinos D & Kondarides I, *J Hazardous Mater*, 372 (2019) 52.
8 Ritika, Kaur M, Umar A, Mehta S K, Singh S, Kansal S K, *Nanosci Nanotechnol Lett*, 9 (2017) 1966.
9 Chen B, Wang B, Sun Y, Wang X, Fu M, Wu J, Chen L, Tan Y, & Ye D, *Catalysts*, 9 (2018) 2.
10 Li H B, Jiang P, Zhang W B, Chen S G & Li F J, *Nanosci Nanotechnol Let*, 11 (2019) 31.
11 Mishra M & Chun D M, *Appl Catal A*, 498 (2015) 126.
12 Bhosale T, Kuldeep A, Pawar S, Shirke B & Garadkar K, *J Mater Sci: Mater Electron*, 30 (2019) 18927.
13 Low J, Cheng B & Yu J, *Appl Surf Sci*, 392 (2017) 658.
14 Zhang B, Cao S, Du M, Ye X, Wang Y & Ye J, *Catalysts*, 9 (2019) 91.
15 Carlucci C, Degennaro L & Luisi R, *Catalysts*, 9 (2019) 75.
16 Etacheri V, Di Valentin C, Schneider J, Bahnemann D & Pillai S C, *J Photochem Photobiol C*, 25 (2015) 1.
17 Vorontsov A V, Kabachkov E N, Balikhin I L, Kurkin E N, Troitskii V N & Smirniotis P G, *J Adv Oxid Technol*, 21 (2018) 127.
18 Weon S, Choi J, Park T & Choi W, *Appl Catal B*, 205 (2017) 386.
19 Tsuji M, Matsuda K, Tanaka M, Kuboyama S, Uto K, Wada, Kawazumi H, Tsuji T, Ago H & Hayashi J, *Chem Select*, 3 (2018) 1432.
20 Jia C, Zhang X & Yang P, *Appl Surf Sci*, 430 (2018) 457.
21 Sing K S W, *Pure Appl Chem*, 57 (1985) 603.
22 Guo C, Ge M, Liu L, Gao G, Feng Y & Wang Y, *Environ Sci Technol*, 44 (2010) 419.
23 Li D & Haneda H, *Chemosphere*, 51 (2003) 129.
24 Dong P, Wang Y, Li H, Li H, Ma X & Han L, *J Mater Chem A*, 1 (2013) 4651.
25 Wang P Q, Bai Y, Liu J Y, Fan Z & Hu Y Q, *Catal Commun*, 29 (2012) 185.